

Nanoliter-Scale Autonomous Electronics: Advances, Challenges, and Opportunities

Authors

Alyosha Christopher Molnar, Sunwoo Lee, Alejandro Cortese, Paul McEuen, Sanaz Sadeghi, and Shahaboddin Ghajari

Affiliation

Cornell University, Ithaca, NY 14853, USA.

Introduction

While CMOS scaling has long been driven by economic and performance concerns in macroscale systems such as computers and smartphones, it has also been recognized that such physically small electronic components could pave the way to vanishingly small autonomous systems. Originally dubbed “smart dust”, these emerging systems include ultra-small wireless sensors, ID tags, and even robots. Such “Smart Dust” was envisioned to be smaller than a grain of sand, yet measuring and reporting signals around it while being powered and communicating entirely wirelessly [1, 2].

However, early autonomous sensors, while leading to a great deal of interesting work in low power radios, power management, and computing, were physically closer to gravel than dust in size (cm’s on a side and milliliters in volume) [3, 4]. Only in the last decade, have sand-grain-scale sensor motes (mm’s on a side and microliters volume) [5, 6], appeared, usually involving heterogeneous stacking of custom ICs and other elements connected with wirebonds and incorporating all the necessary functions of an autonomous node: power harvesting, sensing, signal conditioning, wireless communications, and computing.

Achieving truly dust-scale wireless sensors (100 μ m on a side and <1 nanoliter in volume), however, has taken almost another decade, and have only started to arrive in the past few years. Advancing from the sand-grain to the dust-mote scale requires significant modifications in every aspect of the system. Wireless power and communications change drastically with a 100 \times reduction in surface area and 1000 \times reduction in volume. Furthermore, given that a 100 μ m autonomous IC is the size of a single bondwire pad, assembly and packaging must also be reassessed. This paper discusses the opportunities as well as the technical challenges in developing dust-scale autonomous electronic systems, with the authors’ recent work serving as examples of what is currently possible and what important challenges and opportunities remain.

Benefits and challenges of nanoliter autonomous systems

Extreme size scaling of autonomous systems has the great benefit of making them less disruptive to the environments in which they are deployed. Nanoliter biomedical implants would be much less invasive than their macroscale counterparts, a nanoliter ID tags adds negligible volume and weight even to very small objects or organisms. Small size also reduces per-unit-cost as devices with 100 μ m dimensions can be produced for under a penny apiece [7], while generating far less electronic waste than their macroscale counterparts.

Despite the compelling benefits, the design and the fabrication challenges involved in developing such small systems are far from trivial. The major obstacles in building nanoliter size electronic motes lie in 1) providing them with power, 2) supporting wireless communications to move data on and off of them, and in 3) assembly and packaging.

1) **Power** becomes problematic as there is little room for energy storage (no battery) at such scale, and the power must be delivered wirelessly or scavenged. At the same time, the small volume and surface area of the chip limits how much power can be absorbed from outside, requiring the circuitry itself be extremely low power.

2) **Wireless communication** enables such systems to be tetherless, where wired connections to such small systems are difficult, if usually undesirable. Wireless communications are limited both by the available power and the size of the emitters (for transmission) and absorbers (for reception) of the communication signals (e.g., antennas for radio frequency signals). Fortunately, most nanoliter

motes applications require comparatively low data rates and allow for short distance communications (i.e., out of tissue).

3) **Assembly and packaging** must support heterogeneous integration of elements, such as CMOS circuits and aluminum gallium arsenide (AlGaAs) LEDs, needed for sensing, power harvesting and communications. However, when one’s entire system is smaller than a bondwire, standard assembly techniques cannot be applied. Furthermore, hermetic packaging must not significantly increase the system volume, implying a few μ m thick encapsulation at most, all the while guaranteeing the longevity of such nanoliter motes in harsh environments (i.e., inside the body). Naturally, these challenges favor the heterogenous integration to be as monolithic as possible.

Wireless modalities of micro-to-nano-liter scale motes.

In recent years, three modalities have been investigated for wireless/tetherless power and communications: 1) radio-frequency electromagnetics (RF), 2) ultrasonics (US), and 3) light. Fig. 1. illustrates each modality with an associated circuit interface.

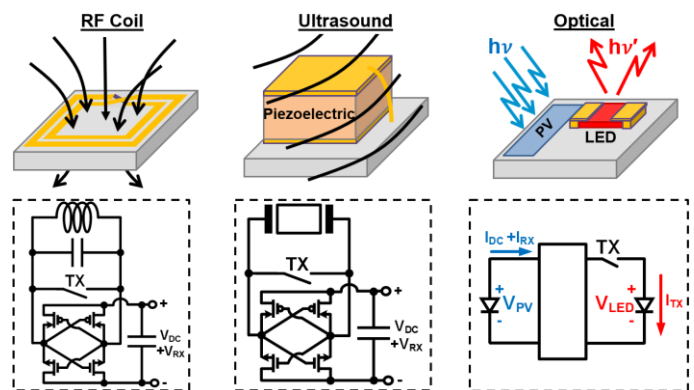


Fig. 1. Common modalities for wireless/tetherless power transfer and data communication in micro- and nano-liter scale motes.

Since micro- and nano-motes’ sizes are well below the wavelength of typical MHz-to-GHz RF signals, wireless power and data transmission using RF usually relies on magnetic coupling through an on-board coil. Indeed, such coils have long been a staple of mm-scale biomedical implants [8] and may be effectively integrated on-chip [9] for fully integrated micro-mote scale sensors. Power and data reception are accomplished with CMOS rectifiers, while data transmission either employs RF transmission or backscatter by modulating the coils load. However, as the coil size shrinks well below one millimeter on a side, it is not only difficult to harvest enough magnetic flux to provide sufficient power, but the coil impedance also decreases, making it difficult to generate enough RF voltage to drive a rectifier. For instance, to generate even a 30mV AC signal from 1 μ W requires \sim 1k Ω coil impedance. Thus, the smallest RF coil-based motes demonstrated are on the scale of 300 μ m on a side [10].

Ultrasonics have also been proposed as a modality for wireless power and data transmission to micro- and nano-liter motes [6]. Importantly, ultrasonics can provide very low loss when the mote is embedded in fluid or tissue. Additionally, the comparatively short wavelength of ultrasound, compared to RF, means that signals can be more effectively directed in tissue, to greater depth, and can be harvested by piezoelectric resonators on the scale of the wavelength. DC power harvesting, data reception, and transmission employ similar rectification and load modulation techniques as RF. Thus, from the perspective of very small biomedical implants, especially when embedded deep in tissue, ultrasonics provide an appealing option. However, at least for demonstrated systems thus far, the required piezoelectric transducers have been many 100’s μ m on a side and hindered by the impedance mismatch between the piezoelectric materials and the tissue.

The third common modality is light. The major benefits for using light (visible or near infrared) is that its wavelength is much shorter than the size of even a nanoliter mote, and the associated efficient transduction of light to electrical power using semiconductor

photovoltaics. Indeed, light has been considered one of the most promising modalities for power and communications ever since “Smart Dust” was first proposed [1]. Clearly, in contexts where a nano-mote must be embedded in an opaque medium, light is not viable. However, most tissue is not so much absorbing as it is scattering, such that nano-motes embedded several millimeters deep in tissue (which may be completely ‘invisible’ due to light scattering) can still be sufficiently powered and communicate through scattered photons [11]. Because it is most suitable for sub-nanoliter-scale wireless motes, the rest of this paper will focus on the challenges and techniques for building optically powered and communicating nano-motes, drawing primarily on our recent work in this space.

Core circuit challenges

Recently, several nanoliter-scale motes using light for power and communications have been presented [11, 12, 13, 14]. Their small size and low power drive unique design requirements and tradeoffs.

Challenges in sensed signal amplification and conditioning:

Nanoliter motes for sensing applications, especially of bioelectrical signals [11, 12, 13, 14], face the tradeoff between input-referred sensor noise and power consumption. The direct relationship between the input referred thermal noise and the bias current (and therefore DC power) in an amplifier is well established [15], providing a limit on achievable noise floor for a given amount of available power. While the severity of this requirement depends on the signals of interest, it is quite constraining for neural recording, where signals are relatively weak (10s μ V) and bandwidth is comparatively wide, for a sensor, at \sim 10kHz. To achieve acceptable noise performance, neural recording motes consume \sim 500nW just for their first amplifier.

A second limitation arises from the trade-off between amplifier size and flicker noise, which can dominate low bandwidth sensed signals. When the entire available area on chip is \sim 10,000 μ m², low-flicker noise, hence large, input transistors can easily consume a large fraction of the available chip space.

Another major challenge concerns the trade-off between impedance, noise, bandwidth, and capacitor size. To avoid noise aliasing in a sampled system, on-chip low-pass filtering is needed, formed by the RC poles in the simplest case. However, achieving a low frequency pole leads to prohibitively large resistors and capacitors when the entire chip is the size of a single 40pF MOS capacitor. Thus, a careful co-design of amplifiers and low-pass filtering is needed to achieve antialiasing within the extreme physical confines of a nano-mote.

This ‘payload’ of nanoliter motes can quickly exhaust most of the available chip area and a significant portion of available power, leaving less for ensuing stages such as communications.

Challenges in optical communication:

The other major power and area consumer in a nanoliter mote is in optical data transmission. The communication range, especially through scattering media (most tissues), depends on providing sufficient emission power, to provide enough photons to receiver. For example, in the context of transmitting through several millimeters of neural tissue, only \sim 0.01% of photons are expected to reach the outside. With a typical detection limit of a sensitive detector, 10-100 photons, this implies 10^5 - 10^6 photons must be emitted just to be detected, let alone support high fidelity decoding [11].

Several optical communication methods have been proposed for such small motes. The simplest is to transduce measured signals directly into light intensity [16], requiring few if any transistors to implement [7]. However, such an approach is susceptible to signal corruption from amplitude fluctuation inherent to the optical path between a mote and an external optical receiver. More critically, this scheme requires the optical signal to be received with an SNR greater than the sensor SNR to avoid corrupting the measured signal.

For analog signals, a far more photon-efficient encoding scheme is pulse-position modulation (PPM). Indeed, PPM is well known to provide the best achievable photon efficiency (in terms of photons per bit of information) when the channel bandwidth is much greater

than the bandwidth of the information being communicated [17]. This is a direct consequence of Shannon capacity:

$$DATE\ RATE < BW \times \log_2[1 + SNR] \quad (1)$$

Even the low average-power circuits of a nanoliter mote can generate current pulses lasting a few 10’s of nanoseconds (corresponding to bandwidths of 10’s of MHz). This is three to four orders of magnitude wider than the bandwidth of most sensor data of interest, allowing much worse SNR, and consequently much lower optical power for a given signal fidelity. For instance, a neural signal with a 10kHz bandwidth and a 40dB instantaneous dynamic range is equivalent to \sim 70kbps, which when mapped onto the 10MHz bandwidth pulses allows an SNR (in average power) of -20dB.

For a simple PPM, the sensor output voltage or current, after low-noise amplification (part of the ‘payload’), is converted into a time delay in a transmitted light pulse. This time delay encoding can be accomplished by driving a current mode signal onto a small capacitor, triggering a pulse when the capacitor voltage reaches a fixed threshold, followed by resetting the capacitor based on an on-chip clock. If the clock’s oscillator is implemented as a similarly structured relaxation oscillator (with current and capacitor proportional to the encoder, and equal threshold voltage), the data is encoded by each pulse’s position as a process-invariant fraction of clock period. Fig. 2. demonstrates an example implementation the approach.

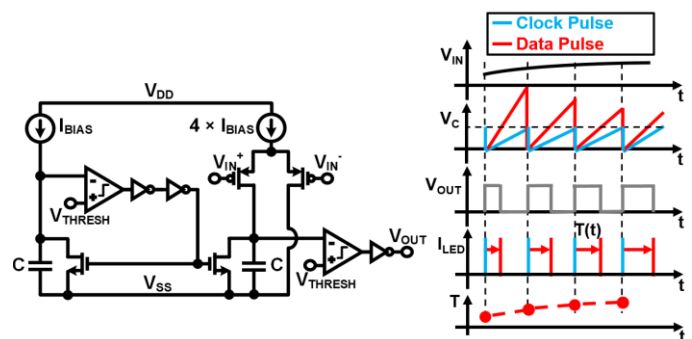


Fig. 2. Example circuit and internal signals for PPM encoder [11].

One major challenge with such an encoding scheme is that it places jitter/phase noise restrictions on the clock to avoid degrading the signal. This puts limits on both how low the power consumption of the on-board oscillator can be and how stable the clock needs to be against power supply fluctuations, etc.

Greater robustness can be achieved by sending a pair of pulses, one based on the reset generated by the on-chip oscillator, the other delayed by an amount set by the encoded signal. Since the critical signal is encoded in the timing difference between pulses, it does not directly reflect jitter in the clock itself, at the cost of $2\times$ reduction in photon efficiency, since two pulses are required per sample. In addition, to avoid unwanted modulation due to power supply variation due to light-level fluctuations, optimal oscillator and encoder designs rely on using a stable current source (from a PTAT or other fixed bias) and a threshold tracking the capacitor reset level.

In cases where data to be sent are already digital (*i.e.*, a bit to indicate an event, or a predefined digital code associated with an event [14]), it can be beneficial to send the bits directly, but the point remains that it is more effective to send bits as the presence or absence of pulses rather than as a weaker, continuous signal of the same average power.

Finally, to generate maximally intense light pulses from continuously sourced external light power, energy must be accumulated slowly and then discharged quickly through the LED to generate a short, bright pulse. One technique to accomplish this is to accumulate charge on a bank of capacitors and to discharge them through the LED quickly. Since power harvested from light on a photovoltaic tends to generate voltages of 1V or less (1V for AlGaAs; 0.4-0.6V for a Si), while an LED needs a higher voltage to emit efficiently, a voltage step-up is also necessary. This can most easily

be accomplished by a switched-capacitor boost converter, where the pulse width is set by the resistance of series switches and the LED, multiplied by the series capacitance of the boost converter. The amount of charge pushed through the LED depends on the PV voltage V_{PV} , the LED turn-on voltage V_{LED} , the total available capacitance C_{tot} , and the number of capacitors N , which also sets the open circuit voltage step up ratio. The charge through the LED is approximately:

$$Q_{LED} = C_{tot} \left(\frac{V_{PV}}{N} - \frac{V_{LED}}{N^2} \right) \quad (2)$$

From this, it can be shown that the optimal step-up ratio, N , for a given total capacitance is the closest integer to:

$$N = 2V_{LED}/V_{PV} \quad (3)$$

One good example of a relatively simple nano-mote sensor is a microscale opto-electronically transduced electrode (MOTE) as shown in Figs. 3 and 4 [11,12]. In this design, the LED (used as an LED about 2% of the time, only while pulsing) also served as the photovoltaic for power harvesting the other 98% percent of the time, such that the optimal step-up ratio in the boost was 2:1 or 3:1 since the V_{LED} was only slightly larger than the V_{PV} .

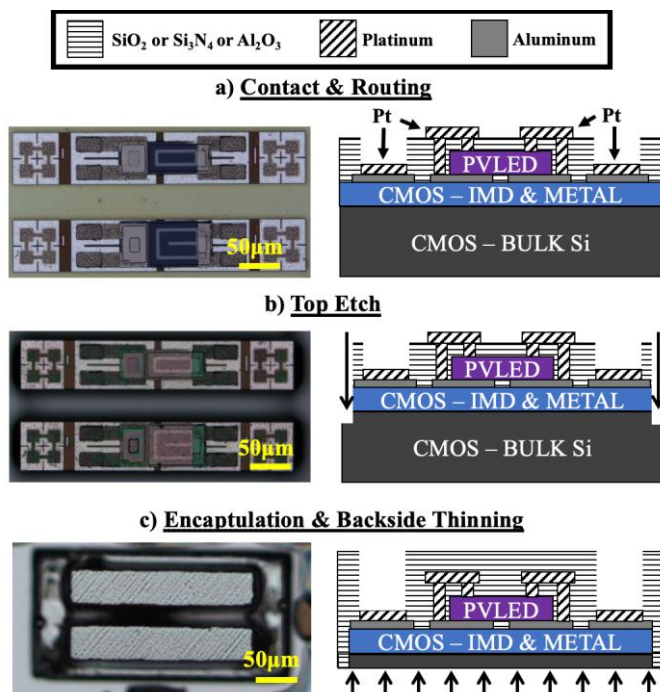


Fig. 3. MOTEs integration fabrication flow [11].

Assembly Challenges and Techniques

Employing light as for power harvesting and communication requires materials that can act as a photovoltaic (PV) and LED. Si used in CMOS circuits can provide the PV functionality with an open circuit voltage of 0.4-0.6V. However, as an indirect semiconductor, Si cannot emit light for communication. Thus, optical nano-motes must combine conventional CMOS with a μ LED made of a direct bandgap semiconductor such as AlGaAs [7, 11, 13], which can also provide a higher open circuit voltage near 1V if used as a PV. The challenge, then, is how to assemble such a μ LED on CMOS.

While it would be ideal to be able to grow AlGaAs directly on top of the CMOS die, the lattice mismatch and required thermal budget make such approach impractical. For the MOTEs in [11,12], AlGaAs μ LEDs are batch fabricated on a sapphire wafer for lattice matching [7], coated in polymer and released from the sapphire to create a μ LEDs array embedded in the polymer. Similar to the techniques used in 2-dimensional (2D) materials transfer [18], the μ LEDs array is then transferred onto the CMOS die and aligned such that each μ LED lines up with the MOTEs' CMOS circuitry. Following this transfer and a subsequent anneal, the AlGaAs μ LEDs are electrically connected to the CMOS die via Pt interconnects [11].

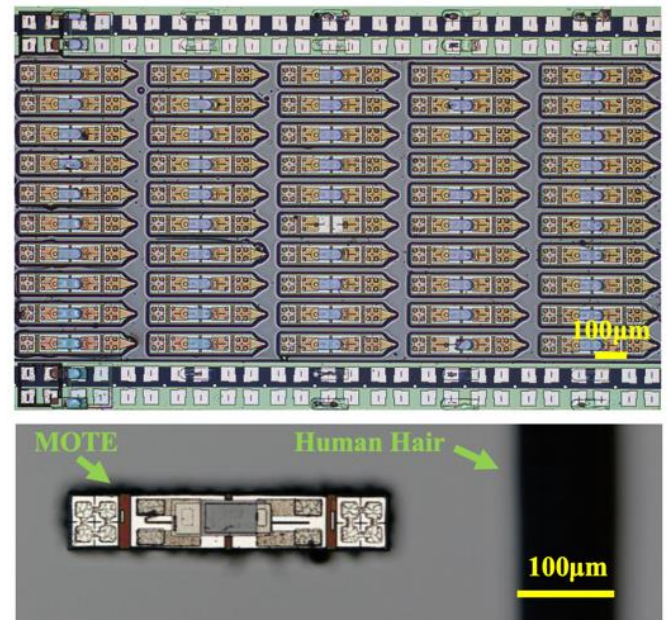


Fig. 4. MOTEs batch fabrication (top) and a fully-released MOTEs compared to a human hair (bottom).

After the heterogenous integration of AlGaAs μ LED and CMOS is completed, the inter-metal dielectric (IMD) and inter-layer dielectric (ILD) of the CMOS are etched to dissociate each unit MOTEs, and the Si around each MOTEs is etched further ($\sim 10\mu\text{m}$), to define maximum MOTEs thickness.

To ensure the longevity of MOTEs-like implants in harsh environments, stable encapsulation is imperative. Furthermore, such encapsulation needs to be minimal in thickness to minimize the total implant size. Atomic layer deposition (ALD) of films in conjunction with plasma-enhanced chemical vapor deposition (PECVD) to deposit alternating layers of SiO_2 , Si_xN_y , and Al_2O_3 where the PECVD films provide appreciable thickness ($< 1\mu\text{m}$) and the ALD films fill in the gaps and pinholes in the PECVD films. The result is the total encapsulation thickness $\sim 1\mu\text{m}$ that can provide sufficient encapsulation for four months (and counting) lifetime of MOTEs inside mouse brains [13].

Following the encapsulation with ALD and PCEVD, the chip is flipped upside down against a carrier wafer to etch the backside Si until the Si trenches isolating each MOTEs appear. The MOTEs are then released into a isopropanol-filled vial. Several of these steps can be simplified if the CMOS circuitry is implemented on a thick silicon ($> 2\mu\text{m}$) SOI, as the buried oxide provides a natural etch-stop during the release from the bulk wafer. Fig. 3. illustrates integration fabrication steps and Fig. 4. demonstrates how the process can be done in batch along with an exemplary fully-released MOTEs.

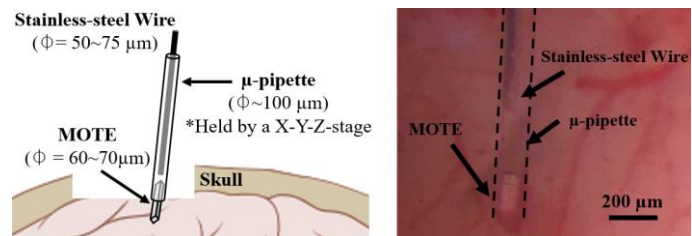


Fig. 5. A MOTEs insertion using a pulled μ -pipette. The left shows a simplified insertion mechanism while the right shows an *in vivo* insertion into the mouse brain [13].

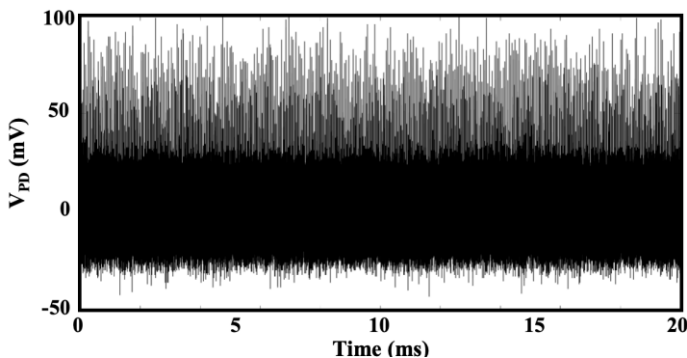


Fig. 6. An *in vivo* measurement of a MOTE implanted in the barrel cortex of a mouse. The observed optical pulses indicate that the MOTE is functioning as designed [13].

An additional difficulty with nanoliter-scale motes is handling: at ~50 μ m or smaller in cross-sectional diameter (smaller than human hair) manipulating and positioning such motes is a challenge in itself. Micropipettes (μ -pipettes), connected to a syringe through a rubber tube, can be used to pick up individual MOTEs using suction to either place them in a desired location, or to directly inject them into tissue through a nanoinjector [13]. Fig. 5. shows such deployment scheme in action and Fig. 6. reports an *in vivo* measurement from a MOTE implanted in a mouse barrel cortex using the nanoinjector method [13].

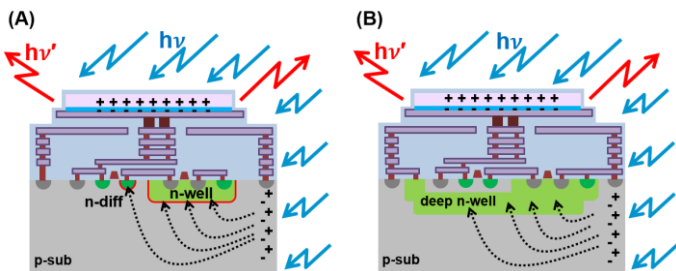


Fig. 7. Photo-generated carriers in deep substrate diffuse to exposed junctions. (A) Carriers generate current in drain diffusions and between V_{SS} -connected p-type substrate and n-well connected to V_{DD} . (B) Deep n-well tied to p-type substrate shields circuits from deep carriers.

Challenge: Stray photo-generated currents

While light provides power for the implant, the same light can also disrupt circuit function, as every junction in the circuitry can also act as a photodiode. Therefore, shielding core circuits from light is vital. To achieve this in the layout of CMOS circuits we have limited routing to the lower metals, so that the upper metals can be mainly used as light shielding. In addition, two walls of contacts and vias are placed all around the circuitry to minimize the ‘leakage’ of light coming in from the side, and placed circuits that are particularly light sensitive (*i.e.*, junctions to high impedance nodes) at the center of the circuit.

Unfortunately, once such nanoliter scale motes are released, light can also disrupt circuitry from other directions. In particular, light striking the silicon substrate from below can penetrate to some depth, especially for longer wavelength light, and so reach circuitry from below. More problematically, light absorbed in the substrate generates electrons and holes that can then diffuse into the circuitry from below, and be swept up by any PN junction the circuit and generate spurious current, generating a variety of problems.

For standard CMOS well biasing, where the p-substrate is biased to V_{SS} and n-wells to V_{DD} , any carriers that reach a p-sub to n-well junction induce leakage current from V_{DD} to V_{SS} . Since n-wells can easily cover half the area of a CMOS circuit, this leakage can be significant and compete with or even overwhelm the current provided by the (intended) PV used to power the circuit. This issue can be

greatly mitigated by using the deep n-well of a triple-well process to effectively “shield” circuitry from below. The deep n-well can be shorted to the p-substrate to shunt any carriers absorbed in this junction, while treating this combined node as “ V_{DD} ”. P-wells inside the deep n-well can then be biased to V_{SS} . This still leaves a reverse-biased p-n junction from V_{DD} to V_{SS} , but this junction is isolated from carriers generated in the deeper substrate. Fig. 7. depicts such impacts of photo-generated carriers and the deep n-well shield approach.

Placing all transistor inside wells also helps against the second problem of photo-generated carriers being absorbed directly by the source and drain junctions of the FETs. While light directly absorbed in the junctions themselves cannot be helped, light absorbed in the surrounding silicon generates carriers that will tend to diffuse into and be absorbed by the nearest junction. Placing all transistors inside wells means that the well junctions themselves will tend to absorb most of the carriers generated in that well, protecting the transistors.

Even with light shielding from above, and well shielding from below, it is difficult to prevent all light from entering the circuit, given the significant light may be needed to power the circuits through a co-integrated PV. Thus, there may always be some extra current leakage across junctions. While these currents can be made very small using the techniques described above, they still can disrupt nodes with very high DC impedances, such as those biased through the pseudo-resistors that are popular in many neural amplifiers [8]. Thus, circuit designs employing such techniques are less reliable in the context of optically powered nanoliter motes and should be avoided where possible. Beyond this, where high impedance nodes are not easily avoided, junction size should be absolutely minimized, placed in minimum size wells, and places as far from the edges of the mote as possible.

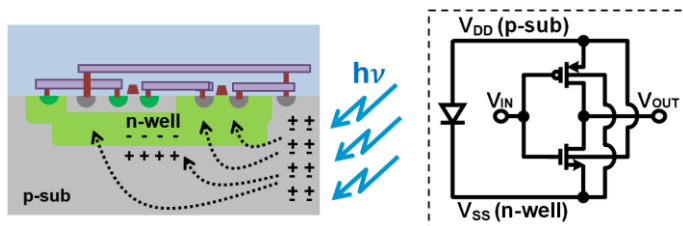


Fig. 8. p-sub n-well photovoltaic power: cross section (left) and schematic of an inverter in such PV-well powered design (right).

Future Directions:

Alternate circuit design methodology: Si bulk as power source

While light leaked into circuits is usually detrimental to their function, it can also be used to harvest power. Surrounding circuitry in deep n-well, as described above, shields those circuits from most photo-generated carriers in the substrate, but can also harvest those carriers for power.

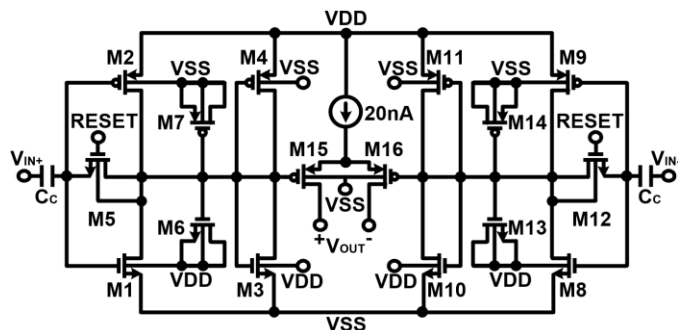


Fig. 9. A Si-PV based amplifier schematic.

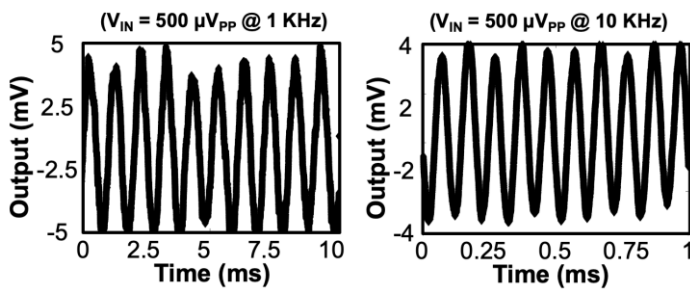


Fig. 10. A Si-PV based amplifier outputs at $V_{DD} = 425\text{mV}$ and $I_{DD} = 1\mu\text{A}$.

Rather than shorting out the deep n-well to p-substrate junction, it can instead be used as an embedded photovoltaic. Since this deep n-well would cover essentially all the circuitry, this approach can employ the entire silicon substrate for energy harvesting. This drives the n-well to a lower voltage than the substrate such that the n-well is now biased to V_{SS} and p-substrate and p-well to V_{DD} . Transistor bulks are therefore partially forward-biased as shown in Fig. 8. Since the open circuit voltage that can be supplied by Si PV is low, this forward bias does not cause significant current to flow through source and drain junctions but does result in a reduction in the threshold voltages of transistors, this can be beneficial, given the relatively low supply voltage provided by the Bulk-based PV.

As an exploratory demonstration of this design approach, we have designed a neural amplifier, similar to the one used in MOTE designs [11], but based on such a bulk-based Si PV power supply ($V_{DD} \sim 0.5\text{V}$ and $I_{DD} \sim 1\mu\text{A}$). Fig. 9 presents a schematic of this amplifier, where M1, M2, M3, M4, M8, M9, M10, and M11 define an inverter-based amplifier with a gm-ratio gain ($>20\text{V/V}$). Input capacitors C_C and pseudo resistors M5 and M12 define the high-pass corner $\sim 10\text{Hz}$, while MOS capacitors M6, M7, M13, and M14 define the low-pass corner $\sim 15\text{KHz}$. It should be noted that all the active transistors bulks are forward biased. Fig. 10 shows an exemplary output from the Si PV-based amplifier, where the amplifier gain is attenuated by a succeeding source follower.

Beyond sensors – ID Tags

One of the next-generation nanoliter motes we are developing is a microscopic optical ID tag. When illuminated with the equivalent power of sunlight ($\sim 1\text{mW/mm}^2$), such a tag blinks out a unique ID code as a series of optical pulses from an integrated microLED. It functions similarly to an RFID tag but is powered by and

communicates with light and has a footprint about $1,000\times$ smaller than most commercial NFC RFID tags.

One such $100\mu\text{m}$ by $150\mu\text{m}$ tag, prior to microLED integration and release from the substrate is shown in Fig. 11. (A). The top third of the tag is composed of silicon photovoltaics for power while the lower two thirds are dedicated to the remaining circuitry and capacitors for driving the microLED. A block diagram of the underlying circuitry is shown in Fig. 11.(B). One set of photovoltaics provides power to the control circuitry while a second isolated set of photovoltaics provides power to the large capacitors that are used to drive the microLED.

Fig. 11. (C) shows electrical measurements of the microLink's output current as a function of time while it communicates out its 64-bit unique ID. The output code is composed of pulses alternating between a timing pulse that is always present and a data pulse that is either present for a binary "1" or absent for a binary "0." The integrated charge in each pulse is about 20pC , which based on previous microLED integration should map to approximately 2×10^6 photons per pulse, easily detectable with mm-scale photodiodes from distances greater than a few cm.

Beyond sensors – microrobots

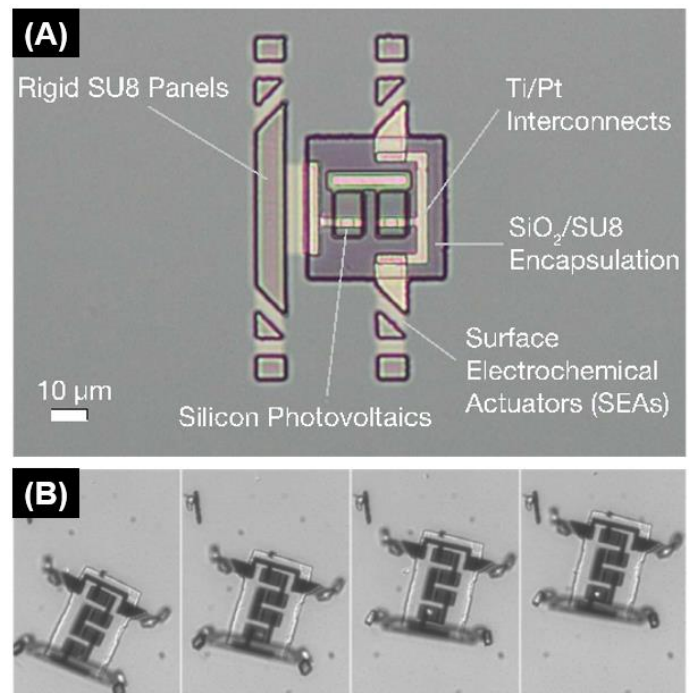


Fig. 12. Electronic microrobots [19]. (A) Optical image of a microrobot. It has two parts: a body with internal electronics and legs that actuate. The legs are made from surface electrochemical actuators (SEAs) and rigid SU8 panels. (B) By directing laser light to photovoltaics that bias either the front or back legs, the robot walks along patterned surfaces.

From the first proposal of smart dust as a concept, a foreseen application has been in microrobots. Such microrobots could be used in a variety of applications, not least of which would be delivery of microsensors to desired target locations. The main additional requirement to convert a nanoliter mote into a nanoliter robot is micron-scale electronic actuators that can seamlessly integrate with semiconductor processing. To meet this need, we developed a new class of voltage-controllable electrochemical actuators that operate at low voltages (200mV), low power (10nW), and are completely compatible with silicon processing [19]. We also developed a full set of lithographic fabrication and release protocols to produce up to one million robots per 4-inch wafer, establishing a clear pathway to mass-

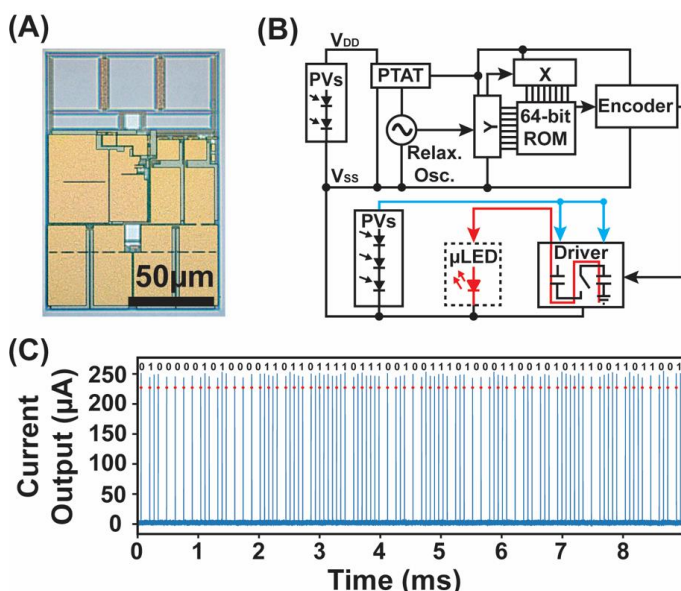


Fig. 11. Microlink nanoliter ID. (A) die-photo, (B) block diagram, and (C) pulsed ID output.

manufactured, increasingly complex and functional cell-sized robots. Fig. 12. (A) shows a simple microrobot still attached to its substrate. The legs of this microrobot are directly driven by a pair of integrated photovoltaics, such that the microrobot walks when illuminated by a sequence of laser pulses, on these PVs as shown in Fig. 12. (B). Combining these techniques with those described above, autonomous, sub-nanoliter microrobots, powered, controlled and communicating with light, will soon be a reality.

Conclusion

The idea of true dust-scale autonomous opto-electronic systems has been discussed for more than two decades. But only in the last few years have techniques in circuit design, nanofabrication, and heterogeneous integration reached the point where such systems are a reality. With a wide variety of possible applications, from biosensors and ID tags to microrobots, such systems present an exciting new frontier for integrated circuit and system designers.

References:

- [1] B. Warneke *et al.*, "Smart Dust: Communicating with a Cubic-Millimeter Computer," *Computer Magazine*, 2001.
- [2] B.A. Warneke *et al.*, "An autonomous 16 mm³ solar-powered node for distributed wireless sensor networks," *IEEE SENSORS*, 2002.
- [3] Chee, Yuen-Hui *et al.*, "PicoCube: A 1cm³ sensor node powered by harvested energy," *ACM/IEEE Design Automation Conference*, 2008.
- [4] Sheets, M *et al.*, "A (6x3) cm² self-contained energy-scavenging wireless sensor network node," *WPMC*, 2004.
- [5] Y. Lee *et al.*, "A Modular 1 mm³ Die-Stacked Sensing Platform with Low Power I²C Inter-Die Communication and Multi-Modal Energy Harvesting," *JSSC*, Jan. 2013.
- [6] D. Seo *et al.*, "Wireless Recording in the Peripheral Nervous System with Ultrasonic Neural Dust," *Neuron*, Aug. 2016.
- [7] A. J. Cortese *et al.*, "Microscopic Sensors using Optical Wireless Integrated Circuits," *PNAS*, April 2020.
- [8] R. Harrison *et al.*, "A Low-Power Integrated Circuit for a Wireless 100-Electrode Neural Recording System," *ISSCC*, Feb. 2006.
- [9] S. Imani *et al.*, "A wearable chemical–electrophysiological hybrid biosensing system for real-time health and fitness monitoring," *Nature Communications*, 2016.
- [10] A. Khalifa *et al.*, "The microbead: A 0.009 mm 3 implantable wireless neural stimulator." *TBioCAS*, 2019.
- [11] S. Lee *et al.*, "A 250 μm × 57 μm Microscale Opto-electronically Transduced Electrodes (MOTEs) for Neural Recording," *TBioCAS*, 2018.
- [12] S. Lee *et al.*, "A 330μm×90μm opto-electronically integrated wireless system-on-chip for recording of neural activities," *ISSCC*, Feb. 2018.
- [13] S. Lee *et al.*, "Fabrication of Injectable Micro-Scale Opto-Electronically Transduced Electrodes (MOTEs) for Physiological Monitoring," *JMEMS*, Oct. 2020.
- [14] J. Lim *et al.*, "A 0.19×0.17mm² Wireless Neural Recording IC for Motor Prediction with Near-Infrared-Based Power and Data Telemetry," *ISSCC*, Feb. 2020.
- [15] M. S. J. Steyaert and W. M. C. Sansen, "A micropower low-noise monolithic instrumentation amplifier for medical purposes," *JSSC*, Dec. 1987.
- [16] K. Ganesan *et al.*, "Sensory Particles with Optical Telemetry," *ISCAS*, 2020
- [17] H. Hemmati *et al.*, "*Proceedings of the IEEE*, Aug. 2011.
- [18] X. Li *et al.*, "Large-Area Synthesis of High-Quality and Uniform Graphene Films on Copper Foils," *Science*, 2009.
- [19] M. Z. Miskin *et al.*, "Electronically integrated, mass-manufactured, microscopic robots," *Nature*, 2020.

Acknowledgement

This work was supported in part by the National Institutes of Health under Grant R21-EY027581 and Grant U01-NS107687, in part by the National Science Foundation under Grant ECCS-1542081, and in part by the National Science Foundation under Grant DMR-1120296. This work was performed in part at the Cornell NanoScale Facility, a member of the National Nanotechnology Coordinated Infrastructure, and made use of the Cornell Center for Materials Research Facilities. This work was performed in part at the Cornell NanoScale Facility, a member of the National Nanotechnology Coordinated Infrastructure (NNCI), which is supported by the National Science Foundation (Grant NNCI-2025233).